

Figure 7.9: Mesh details of the experiment steam drum; Coloured by volume size, (a) steam drum, (b) steam drum stage 1, (c) distributor pipe, (d) orifice pipe; figure by the author

### 7.1.2 Steam Drum Simulation Boundary Conditions

The experiment steam drum have a water and an air mass flow inlet, see figure 7.3.

The downcomers and the drum sides are pressure outlets. Whereas the side outlet relative pressure is 0 Pa and the relative pressure at the downcomers depends on the water level in the drum. The pressure at downcomers can be calculated by  $\Delta p_{downcomer} = \rho_{water} g \Delta h_{waterlevel}$ . But during the simulation

run there are different water levels in the turbulent and the calm stage, which is unknown at the beginning. Hence it is a iterative process to find the correct  $\Delta h_{waterlevel}$ , which correspond to the measured water level in the experiment. Due to the unequal water distribution in the feeding pipes the water level is skewed in turbulent section of the experiment drum. The water level scale is on the right side of the baffle plate, like mentioned above. Hence a filter function in the CFD model is needed which return the water level in stage 1 next to the right baffle plate. In the CFX CEL expression language a volume average of the interface height can carried out. At first a CEL function is used to return the y values of interface cells on the right of stage 1 based on the free surface blend function:

Listing 7.1: Y values of right side interface cells CEL expression

```
NOW interfaceYCalm = if( z > -222 [mm] , if( z < -157 [mm] ,
if( x < 63[mm] , if( x > 30[mm] , if( y > -50[mm] , if(
Gas.AV AIAD FS Blend Func > 0.8, Y Coordinate , 0[mm]) ,
0[mm] ) , 0[mm]), 0[mm]), 0[mm]), 0[mm])
```

and the volume of the corresponding interface cells:

Listing 7.2: Volume of right side interface cells CEL expression

```
NOW interfaceVolumeCalm = if( z > -222[mm], if( z < -157[mm
], if( x < 63[mm], if( x > 30[mm], if( y > -50[mm], if(
Gas.AV AIAD FS Blend Func > 0.8, Volume of Finite Volumes
, 0[m^3]), 0[m^3]), 0[m^3]),0[m^3]),0[m^3]),0[m^3])
```

In the second step, both CEL functions in listing 7.1 and 7.2 are defined as additional variables, so that these additional variables can be used in a CEL expression to calculate the volume average interface height:

Listing 7.3: Volume averaged interface height CEL experession

```
NOW waterLevelAve = volumeInt(Gas.AV NOW interfaceY)@fluid /
sum(Gas.AV NOW interfaceVolume)@fluid
```

Subsequently the CEL expression "NOW waterLevelAve" can be monitored during solver run and should correspond to the experiment water level height.

The steam drum outlet is also included in the experiment steam drum for further experiments, but have no task for this thesis and is closed in experiment and defined in the CFD simulation as a wall.

### 7.1.3 Steam Drum Simulation Initial Conditions

The water level in the experiment is about 21.5 mm. But the water content in the feeding pipes are transient and unequal distributed. Hence only stage 1 and 3 of the CFD drum is initialised with a water level of 21.5 mm. The feeding pipe region is initialised with a homogeneous volume fraction. These volume fractions correspond to an ideal mixture of the supplied air/water mixture.

For stability reasons an initial hydrodynamic pressure is needed:

$$p_{init} = (y_{waterlevel} - y) \ g \ \varrho_{mix} \quad (7.1)$$

whereas  $p_{init}$  is only applied in stage 1 and 3 below the water level, else it is set to 0 Pa.

## 7.2 Steam Drum Simulation

This steam drum simulation comparison based on the Schreiber, Hellwig, and Nowitzki (2017) experiment with an air volume flow of  $25 \text{ m}^3/\text{h}$  and a water volume flow of  $500 \text{ L/h}$ . The water level, as well as the droplet mass flow out of the drum sides is monitored in the simulation. Whereas the water level monitor is necessary to control the downcomer pressure boundary condition, see section 7.1.2. The droplet mass flow at drum sides correspond to the measurement results in table 7.1. Like mentioned above the physical set-up is equal validation case FV\_170 and case FV\_190. Hence there are a consistent comparability of Fabre, Masbernat, and Suzanne (1987), Hewitt and Owen (1987) and steam drum simulations.

In general it can be said that with a physical timescale of  $5\text{e-}4 \text{ s}$  the solver run stable and the momentum imbalances are every time in between  $+/- 1\%$ . Sometimes conditions are formed in the simulation, which causes instabilities. These instabilities could not be reconstructed, because within only one iteration the solver crashes. In this short period it is almost impossible to write out a backup file, which can be examined. In addition these instabilities are disappeared after a rerun. It is assumed, that a high gradient value occur on the border between two cpu mesh regions in a parallel run, see keyword "overlap relaxation fluids" in section 5.1.3. But despite of a reduction of the "overlap relaxation fluids" value, the solver crashes again. Only a reduction of the advection scheme specific blend factor to 0.5, the solver runs stable every time. But unfortunately a reduction of the specific blend factor reduce the accuracy of the simulation, see table 5.9.

Before the droplet mass flow can be examined in the simulation, the average water level have to be 21.5 mm below the drum centre line, like in the steam drum experiments. If the water level condition is achieved, the droplet mass flow averaging can be started at this point. As in the other simulations, average values are averaged over 10.000 iterations. The simulated average values of the droplet mass flow out of the sides can be seen in table 7.4.

In Table 7.4 the droplet mass flow at drum sides, the normalised RMS droplet

Table 7.4: Steam drum simulation droplet mass flow at sides; water volume flow  $0.5 \text{ m}^3/\text{h}$ , gas volume flow  $25 \text{ m}^3/\text{h}$ , 1 atm

		Droplet mass flow	NDMFD	abs deviation
		[kg/s]	[-]	[kg/s]
FV_170	left	1.96e-07	0.92	2.12e-06
	right	7.29e-08	0.85	4.29e-07
FV_190	left	4.39e-08	0.98	2.76e-06
	right	2.09e-07	0.58	2.93e-07

mass flow and absolute deviations are shown for the left and right drum side. The normalised RMS droplet mass flow deviation is defined as:

$$NDMFD = \frac{\sqrt{(\Phi_{d,exp}^M - \Phi_{d,sim,ave}^M)^2}}{\Phi_{d,exp}^M} \quad (7.2)$$

The absolute simulation results are close to the experiment results. This can be seen in table 7.4 column absolute deviation. It is evident, that relative deviations are increased, if simulation values are converged to zero, due to numerical fluctuations. Hence the relative droplet mass flow deviation are high.

Generally one condition in order to use this simulation model in an industrial application is, that the simulation produce every time conservative results. In table 7.4 one can see that this condition is violated. Every simulation result is smaller than the corresponding experiment value.

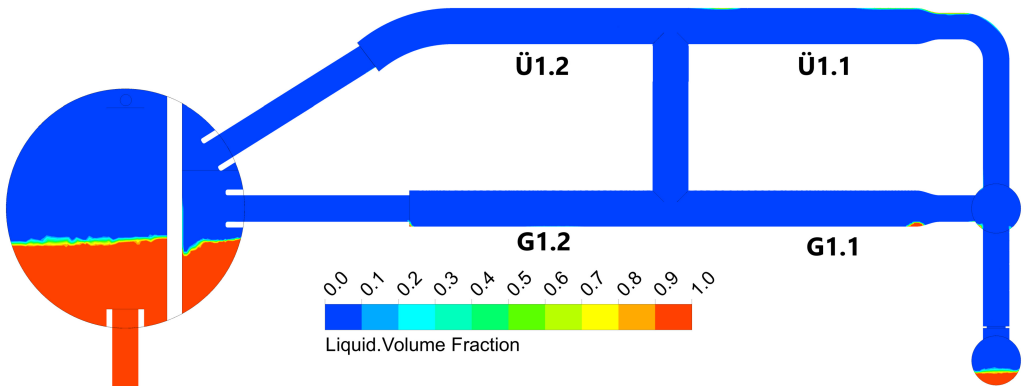
If one compare the different simulation set-ups, the best simulation result is at FV\_190 right side, with a NDMFD value of 0.29. But on the other side the worst simulation result is also at FV\_190 on the left side, with a NDMFD value of 0.98. But the simulation model FV\_170 show the correct ratio between the droplet mass flow at the left and right side. Like mentioned in table 7.1, there is an increased droplet mass flow at the left side compared to the right side. Therefore the simulation model set-up FV\_170 is recommended for steam drum simulations.

In order to compare the experiment with the simulation water fraction, cut planes through the centre of all feeding pipe sets are carried out. In figure

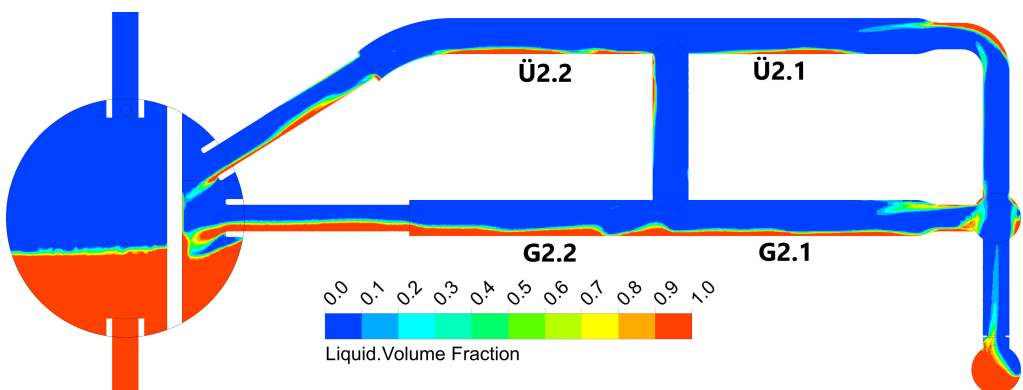
[7.10](#) one can see the cut planes, which are coloured with the liquid volume fraction.

The unequal water content distribution in the experiment can be reproduced by the simulation. In the simulation the water content in the feeding pipes is increased from set 1 to 3 like in the experiment. This is an effect of the inlet condition of the orifice pipe.

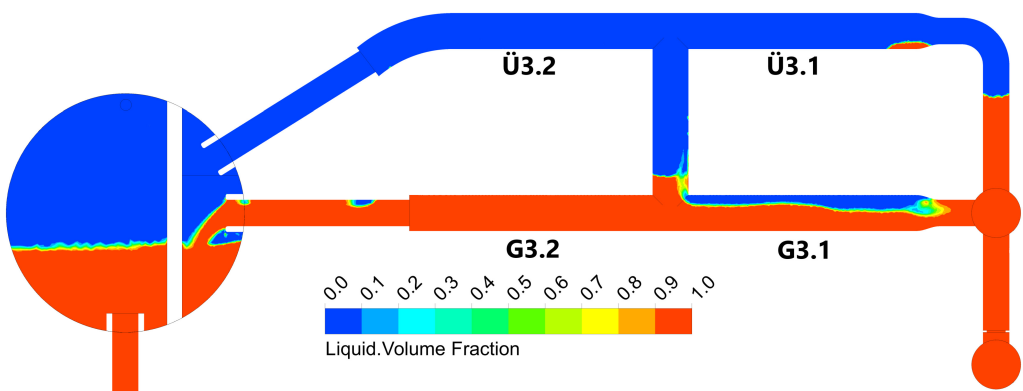
Due to the video recordings it is possible to compare the water content in the feeding pipe set 3 in the experiment and simulation. In order to compare qualitative the water content in the experiment the snapshot in figure [7.4](#) is edited. In these photos the water phase, in light grey, is highlighted. By comparing figure [7.4](#) (a) with figure [7.10](#) G3.1 the flow pattern looks similar. Also the flow pattern in figure [7.4](#) (b) is similar to the figure [7.10](#) G3.2. Though in the experiment there is a clearly recognisable water content in the overflow pipes, see figure [7.4](#) (c) and (d). This water content in the overflow pipes can not be reproduced by the simulation. In figure [7.10](#) Ü3.1 and Ü3.2 there is no noticeable water.



(a)



(b)



(c)

Figure 7.10: Experiment steam drum simulation; Coloured by liquid volume size, feeding pipe (a) set 1, (b) set 2, (c) set 3; figure by the author

## 7.3 Steam Drum Simulation Conclusion

Alone if one take a look at the flow pattern in the feeding pipes, it is evident how complex such a two-phase flow in a steam drum is. The feeding pipes and the steam drum form a system of communicating pipes. Local inaccuracies cause changes in the whole pipe system. Also small inaccuracies of the interface momentum balances has a strong impact of the air/water mixture distribution.

It can be seen in the experiment and the simulation, that the flow pattern in the feeding pipes have a strong impact on the droplet mass flow at the drum sides. That is why it is important for the simulation model to reproduce this flow pattern in the feeding pipes. In order to reproduce the flow pattern, the momentum transfer between both phases should be reproduced exactly. A comparison of the flow pattern in the experiment and simulation mixture pipes set 3, show a good agreement. Though the water content in the simulation overflow pipes in set 3 is less than in the experiment. So that to less water is pushed to the overflow pipes.

It is likely, that is in the third vertical orifice pipe branch a too low gas volume fraction. Hence there are not enough larger bubbles to push the water phase upwards, to the overflow pipes. The orifice pipe is responsible for the air/water distribution of the feeding pipe sets. In figure 7.11 one can see the air/water distribution in the orifice pipe and feeding pipe set 3.

The detail in figure 7.11 show the reason why not enough air can reach the feeding pipe set 3. There are only water on the end of the orifice pipe which create an free surface next to the second branch. The air phase can not overcome this free surface, because the kinetic energy is too low in the free surface region. A model of the free surface region is shown in figure 2.16. The kinetic energy in the free surface region depends on the characteristic length scales and the turbulence damping coefficient.

The characteristic length scale for the free surface region include bubble and droplet sizes, as well as the characteristic length of the free surface itself. That the bubble and droplet sizes play a role for the free surface

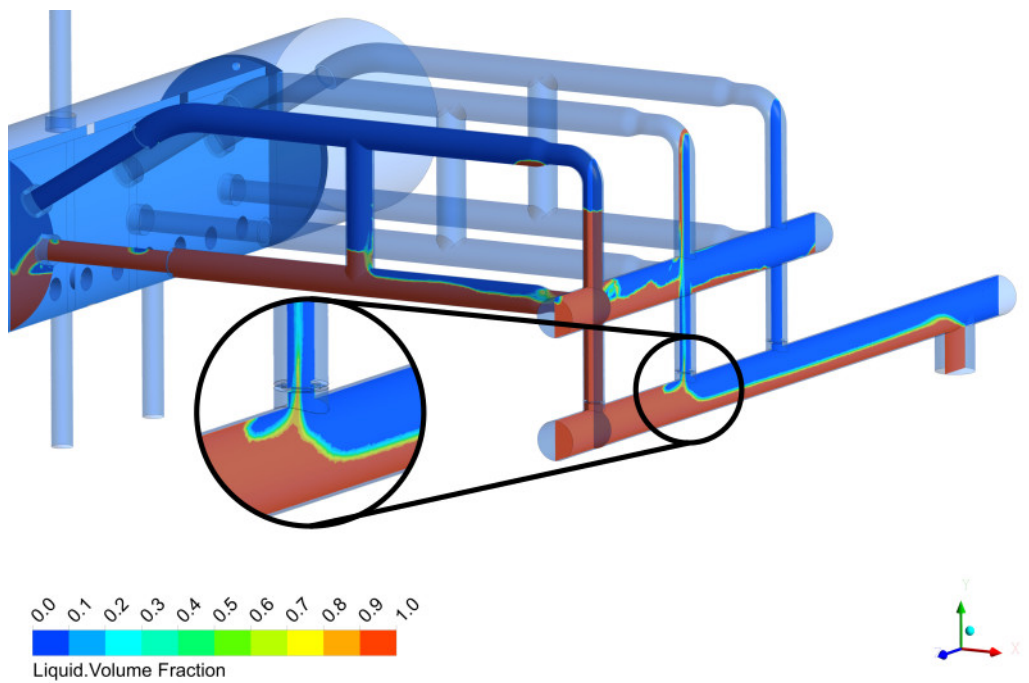


Figure 7.11: Experiment steam drum simulation; Coloured by liquid volume fraction; cut planes through orifice pipes and feeding pipe set 3 and a detail of phase separation in orifice pipe; figure by the author

region is because the blending functions have a slope, see figure 2.15 and the blending function overlap in the free surface region. The free surface region in the simulation is only a model. In reality this region is very thin and it is very hard to measure flow properties and particle distributions close to this free surface. Hence there a lack of experiments and knowledge of characteristic length scales close to the interface. Thus it is difficult to validate the particle size distribution. In the free surface region it could be, that the new particle size prediction model, has an increased deviation, because there are some additional physics, which can be neglected far away from the interface. For example the stronger particle interaction due to the increased density of particles. On the one hand it is possible to include additional models, which take into account these stronger interaction nearby the interface in the algebraic simulation model or a transport equation is used with included particle breakup and coalescence models.

Regarding this transport equation, there are some research approaches to model the phase interaction of a dispersed phase and a continuous phase, namely a mono-dispersed approach with a transport equation for the interfacial area density and a poly-dispersed approach, see Pellacani (2012). In the poly-dispersed approach some additional transport equations are needed and is therefore neglected, due to the high computational time. But the poly-dispersed approach is superior the mono-dispersed approach. The best performance for an industrial simulation could be reached with the interface area density transport equation combined with the mono-dispersed approach. With this latter approach the particle distribution accuracy could be increased, without a significant increase in computing time.

So that the only highly experimental uncertainty is the turbulence damping coefficient, which is not fully understood until today. To overcome this uncertainty more experiments, which examine the turbulence close to a interface is needed. Without a better understanding of the turbulence damping, a validation for every new simulation case is recommended.

Despite of the deviations of the flow pattern in the overflow pipes, the prediction of the mass flow out of the sides are close to the experiment. That implies a good agreement between the modelled droplet behaviour and the experiment. But this determination is only valid for a air/water mixture. But before to use this simulation model as a design tool for industrial steam/water applications, it is necessary to fit some parameter, that the droplet mass flow is every time above the measured values. Recommended fitting parameter are the RRSB scale parameter correction and the turbulence damping coefficient. Further experiments should be carried out with a steam/water mixture to make sure that the simulated steam/water behaviour is close to the experiment also.

Important for industrial application is besides the stability and conservativeness also the computational time. The experiment steam drum simulations takes around 2 days for 9 Mio cells on 40 cores. The reason of this long computational time is mainly the slow adjustment of the water level and thus the mass imbalance convergence. Thus with a better approach to force the

water level adjustment in the steam drum, the overall simulation time will be decreased. Additional in all simulation a large set of CFL expressions are used. These CFL expressions are easy to use but decelerate the solver speed. An implementation of all functions in CFX subroutines would accelerate the solver. Because "Monitor Statistics" in CFX is used, "Mesh Adaption" must be omitted. If the "Mesh Adaption" can be used, the simulation time can be reduced also. With the three above mentioned improvements, the simulation time could be reduced by about a half.

The steam drum simulation had shown, that such a complex simulation can be carried out within a short time with a prediction of droplets in the gas phase close to the experiment. Though for new applications and fluids, validations are needed, which increase the reliability.

# Chapter 8

## Conclusion and Discussion

Simulations of two-phase air/water flows have been performed by means of the two-fluid inhomogeneous Euler-Euler approach. With the AIAD model a morphology detection is implemented. The AIAD model use a mono-disperse approach to determine the interfacial area density for the dispersed phases, in which the average particle sizes need to be known a priori. A new model is implemented in Ansys CFX to estimate the particle sizes, without increase the set of differential equations, which replaces the constant particle size diameter of the AIAD model. State of the art and State of science models, to improve the accuracy of the two-phase interaction, have been added to the CFD model. To these additional models belong the Ishii-Zuber drag model for the dispersed phases and non-drag force models.

The CFD model has been applied to the Fabre experiment. In this analysis combinations of different distributions functions as well as different RRSB model parameter have been tested. In the next step, based on the distribution function analysis results, the impact of submodels and different submodel parameters are examined, on the same Fabre experiment. The best model set-up is tested in a proof of concept for a 3D vertical two-phase pipe flow. In the end a CFD simulation has been carried out of a steam drum, with the CFD model set-up tested before. This steam drum experiment was developed to test the capability of droplets prediction of the two-phase CFD model and carried out at the same time as this thesis. The steam drum experiment is

modified regarding a real industrial steam drum, in order to determine the droplet mass flow which carried away by the air, from the turbulent steam drum region.

The main goals of these analyses is to validate the correct implementation of the submodels, analyse the impact of the submodels on the pressure field, velocity fields and phase distribution, as well as the reproduction of the flow phenomena in the steam drum turbulent region. The steam drum simulation should also demonstrate if the CFD model is able to perform an industrial size steam drum simulation.

Generally, despite of the relative coarse mesh and the wall function approach, the CFD model is able to reproduce a stratified flow in horizontal as well as bubble and plug flows in vertical pipes. Relative pressure deviations are in range of about 0.13 in case FV\_190 to 0.25 in case Hewitt Run 1.

The Fabre simulations pointed out, that the largest deviations between simulation and experiment is regarding the turbulent kinetic energy, see figure 5.9. That the simulation results strongly depends on the turbulence model, can also be seen by the simulation with different turbulence models. To test the turbulence model dependency, a Very Large Eddy Simulations (VLES) has been carried out. This VLES is closest to the results of the Fabre experiment, without distribution function correction factors. But the VLES has been discarded, because of the strongly increased computing time. Hence correction factors are introduced, to enhance the simulation results. Regarding the SST turbulence model, the largest deviation of the kinetic energy is in the free surface region. Which implies, that the particle diameter and/or the "High Turbulence Damping Coefficient" is not adjusted well. Thus correction factors are introduced to adjust the CFD simulation to the Fabre experiment.

Larger deviations have been occurred for higher water content in vertical pipes. While in Hewitt run 6 good results are achieved, deviations between the simulation and the experiment are greater in Hewitt run 1. This discrepancy is probable an interface structure phenomenon. In Hewitt Run 6 there is a plug flow with large interface structures and in Hewitt Run 1 a bubble

flow occur with small interface structures. Hence it could be that the mixture model can not reproduce very fine flow pattern structures like in bubble flows and the prediction of the interface area density becomes inaccurate.

As mentioned in section 7.3 the kinetic energy is important to reproduce the flow pattern. In the steam drum simulation figure 7.11 one can see the similar problem of to low kinetic energy to reproduce a flow pattern with smaller interface structures. The problem can be traced back probably of the inaccurate reproduction of particle sizes in densely particle regions. The accuracy could be increased by an additional transport equation for the interface area density. In this transport equation particle coalescence and breakup is included, see Pellacani (2012). Validation of this model could be carried out with a new feeding pipe experiment or with a simulation with a poly-dispersed approach for the particle distribution.

Good agreement with the experiment results could be achieved for sparsely particle region like in steam drum turbulent region or Hewitt Run 6 case.

Though if the particle distribution correction factor and turbulence damping coefficient adjust to the kinetic energy profile measured by Fabre, Masbernat, and Suzanne (1987), the water carry over to the air is too high. But with this model set-up, which achieve a good approximation of the kinetic energy in the Fabre channel, the flow pattern in the feeding pipes are closer to the steam drum experiment, compare figure 8.1 with figure 7.4.

This advanced steam drum simulation shows, that a well-chosen combination of particle size and turbulence damping coefficient is suitable to reproduce the flow pattern in the feeding pipes, but a too high liquid volume fraction in the air phase is the consequence. In this advanced simulation the droplet mass flow on the left side is about 2.4e-04 and on the right side 3.6e-04. It is probably due to a too strong numerical diffusion of the mixture model approach. To analyse this model diffusion effect the droplet distribution above the interface have to be known. An experiment which provide such a droplet distribution in a pipe or channel is unknown to the author. One possibility to enhance the mono-dispersed approach could be, a validation with the poly-dispersed approach with the Euler-Euler particle model, because this

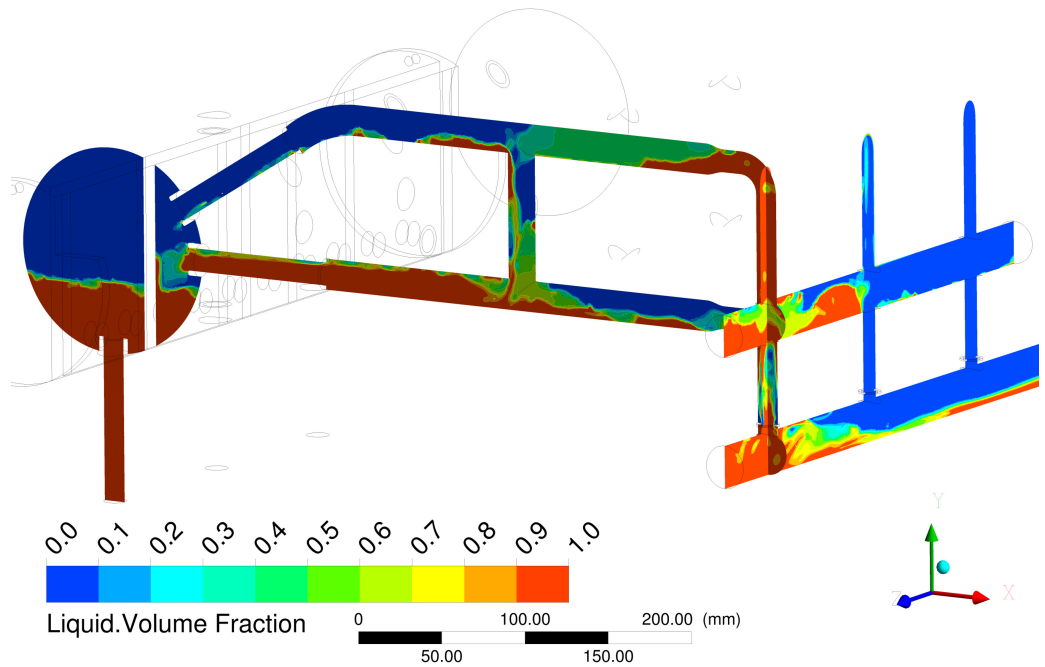


Figure 8.1: Experiment steam drum simulation; Coloured by liquid volume fraction; Cut through orifice pipe and feeding pipe set 3; Advanced interface interaction; figure by the author

poly-dispersed model can better reproduce such droplet distribution above the interface.

To design new or advanced steam drum internals the inlet velocities, inlet steam quality, flow pattern and interface positions have to be known. Until today these mentioned values before are rough estimated or unknown, so that an experiment for every design is needed to examine the separation performance. The simulation model with the Ishii-Zuber drag force and several non-drag forces and with the particle reconstruction model on basis of the AIAD model, can provide these needed values for a separator design process. In the steam drum simulations it can be seen, that the accuracy of the steam quality should be further improved, but the velocities, the flow pattern and the water interface positions can be reproduced with industrial accuracy. Therefore the examination of the steam drum behaviour under worst case scenarios or changing loads is now possible to simulate. Addition-

ally, separator design optimisations can be carried out now on the computer in a shorter time. That allowed the development of new steam drums, which are more suitable for a flexible boiler operation. These new developments would better provide the electrical grid stability with an increased amount of renewable energy technologies.

## Future Work

To increase the reliability of the simulation model, tests with a steam/water mixture should be carried out. It is recommended to design an experiment with only the feeding pipe system and a steam/water mixture. So a feeding pipe simulation is much faster for such a system compared to a steam drum simulation, because the slow mass balance convergence of the drum water level would not exist. It becomes apparent that the flow pattern in such a pipe system is very sensitive regarding two-phase interaction inaccuracies and hence it is a good test case for a simulation model phase distribution. Additional simulations with VLES or LES should be carried out to cancel out turbulence model inaccuracies and adjust the turbulence damping coefficient. Like mentioned above transport equations for the interface area density could be included in the simulation model. This extended model should offer the best compromise between accuracy and computational time.

Like mentioned above, instead of carry out an experiment, it could be possible to build up two simulations based on the Euler-Euler poly-dispersed approach. One simulation with liquid as the dispersed phase and one simulation with gas. This poly-dispersed approach should reproduce the particle distribution in more detail. So the mono-dispersed model can validated with these poly-dispersed simulations. But an experiment is rather recommended.

# Nomenclature

## Acronyms

AIAD	Algebraic Interfacial Area Density
CDF	Cumulative distribution function
CEL	Command Expression Language; Interface in Ansys CFX software
CEL	Ansys CFX command expression language; program user interface
CFD	Computational Fluid Dynamics
CFX	CFD software from Ansys
ERK	ERK Eckrohkessel GmbH
FAD	Favre Averaged Drag
FDBR	Fachberband Dampfkessel-, Behälter- und Rohrleitungsbau e.V.
FVM	Finite-Volume-Method
HZDR	Helmholz-Zentrum Dresden Rossendorf
IAD	Interfacial area density
ILS	Interface length scale
iMUSIG	Inhomogeneous multiple bubble size group model
KH	Kelvin-Helmholtz

KHRT	Kelvin-Helmholtz Rayleigh-Taylor Hybrid model
LES	Large Eddy Simulation
NDMFD	Normal Droplet Mass Flow Deviation
NOW	In this thesis developed model
PBE	Population balance equation
PBM	Population balance model
PDF	Particle size distribution
R&D	Research and development
RMSD	Root mean square deviation
RRSB	Rosin, Rammler, Sperling and Bennet Distribution
RT	Rayleigh-Taylor
SMD	Sauter mean diameter
TDF	Triangle distribution function
UDF	Uniform distribution function
VLES	Very Large Eddy Simulation
VOF	Volume of fluid model

### Greek Symbols

$\alpha$	Angle between pipe axis and the horizontal; positive downward	$^{\circ}$
$\beta$	$k - \omega$ turbulence model constant, according Ansys (2016c)	$-$
$\Delta t$	Time interval	s
$\delta$	interface thickness	m
$\epsilon$	Turbulence eddy dissipation	$\text{m}^2/\text{s}^3$

$\lambda$	Second viscosity = $-\frac{2}{3}\mu$ (Stokes hypothesis), see Anderson (1995)	
		Pa · s
$\lambda$	Wave length	m
$\mu$	Dynamic viscosity	Pa · s
$\nu$	Kinematic viscosity	m <sup>2</sup> /s
$\nu_{turb}$	Turbulent or eddy kinematic viscosity	m <sup>2</sup> /s
$\Phi^M$	Mass flow	kg/s
$\Phi^V$	Volume flow	m <sup>3</sup> /s
$\sigma$	Surface tension	N/m
$\sigma_{turb}$	Turbulent Schmidt number for volume fraction	—
$\tau$	Viscous stress tensor	Pa
$\tau_{turb}$	Turbulent stress tensor	Pa
$\Delta$	Difference of a variable	—
$\Pi$	Pi number	—
$\varrho$	Density	kg/m <sup>3</sup>

### Roman Symbols

$Bo$	Bond number, see Eo	—
$Eo$	Eötvös number or sometimes called Bond number Bo	—
$Mo$	Mortion number	—
$Re_p$	Particle Reynolds number	—
$\gamma$	Distorted fluid particle distortion factor	m
$\vec{F}$	Force	N

$\vec{f}$	Mass specific volume force	N/kg
$\vec{g}$	Gravity acceleration vector	m/s <sup>2</sup>
$\vec{r}$	Position vector	m
$\vec{t}$	Stress vector normal to free surface	N/m <sup>2</sup>
$\vec{t}_{fs}$	Free surface tangential shear stress vector	N/m <sup>2</sup>
$\vec{U}$	Velocity vector	m/s
$A$	Area, Surface	m <sup>2</sup>
$A_{\alpha\beta}$	Interfacial area density; interfacial area per unit volume between phase $\alpha$ and phase $\beta$	1/m
$a_b$	AIAD model constant for bubble regime	—
$a_d$	AIAD model constant for droplet regime	—
$B$	$k - \omega$ interface damping model parameter	—
$B_v$	Steam volume strain	m <sup>3</sup> /(h · m <sup>3</sup> )
$C_D$	Drag coefficient	—
$c_g$	AIAD parameter	m
$C_{RT}$	Adjustable constant for RTB model, see Reitz and Beale (1999)	—
$C_{TD}$	Multiplier for FAD drag model	—
$cp$	Specific heat capacity at constant pressure	J/(kg · K)
$d$	Diameter	m
$d_{32}$	Sauter mean diameter	m
$d_H$	Maximum horizontal dimension of a distorted fluid particle	m
$d'_{p,RRSB}$	Scale parameter in RRSB distribution	m

$d_V$	Maximum vertical dimension of a distorted fluid particle	m
$E$	Aspect ratio of a distorted fluid particle	—
$e$	Mass specific internal (thermal) energy	J/kg
$E_f$	Aspect ratio frontal part of a distorted fluid particle	—
$f$	Blending function in AIAD model	—
$h$	Mass specific enthalpy	J/kg
$K$	Angular wave number	1/m
$k$	Thermal conductivity coefficient	W/(m · K)
$ke$	Kinetic energy	—
$L$	Characteristic length	m
$M$	Indicator function	—
$M$	Mass	kg
$mf$	Mass fraction	—
$N$	Count	—
$n_{RRSB}$	Shape parameter RRSB distribution	—
$NKED$	Normalised kinetic energy deviation	—
$NPGD$	Normalised pressure gradient deviation	—
$NVD$	Normalised velocity deviation	—
$NWLD$	Normalised water level deviation	—
$p$	Pressure	Pa
$q$	Steam quality	—
$S_h$	Volume specific heat source	W/m <sup>3</sup>

$S_{Mass}$	Interfacial mass source	kg/m <sup>3</sup>
$S_{Mom}$	Interfacial momentum source	N/m <sup>3</sup>
$S_M$	Volume specific momentum source	N/m <sup>3</sup>
$S_{st}$	Mixture momentum source due to surface tension	N/m <sup>3</sup>
$t$	Time	s
$u$	Velocity x component in cartesian coordinate system	m/s
$V$	Volume	m <sup>3</sup>
$v$	Velocity y component in cartesian coordinate system	m/s
$vf$	Volume fraction, void fraction	-
$w$	Velocity z component in cartesian coordinate system	m/s
$We$	Weber number	-
$x$	Cartesian coordinate system x coordinate variable	m
$y$	Cartesian coordinate system y coordinate variable	m
$y_W$	Nearest wall distance	m
$YH$	Cumulative distribution function	-
$yH$	Probability density function, Relative frequency	-
$z$	Cartesian coordinate system z coordinate variable	m

### Superscripts

*	Modified
B	Basset
D	Drag
L	Lift

T	Turbulent dispersion
V	Virtual mass
W	Wall-lift or wall-lubrication

### Subscripts

$\alpha$	Fluid identifier; continuous phase
$\beta$	Fluid identifier; dispersed phase
$\gamma$	Fluid identifier
$\infty$	Single particle in infinite media
<i>abs</i>	Absolute value
<i>ave</i>	Average; in steady state 10.000 iterations; in transient 10 seconds
<i>b</i>	Bubble
<i>c</i>	Continuous phase
<i>crit</i>	Critical
<i>d</i>	Droplet
<i>disp</i>	Dispersed phase
<i>eff</i>	Effective
<i>exp</i>	Regarding experiment
<i>fc</i>	Forced convection
<i>fs</i>	Free surface
<i>g</i>	Gas phase
<i>i, j</i>	Control variable
<i>K</i>	Sphere

<i>k</i>	Control variable for phases
<i>K, Veq</i>	Volume equivalent
<i>l</i>	Liquid phase
<i>lim</i>	Limit
<i>m</i>	Mode of particle distribution
<i>max</i>	Maximum
<i>min</i>	Minimum
<i>mix</i>	Mixture
<i>p</i>	Particle
<i>par</i>	Regarding particle model
<i>proj</i>	Projection
<i>ref</i>	Reference
<i>rel</i>	Relative
<i>RRSB</i>	Regarding RRSB distribution
<i>RT</i>	Rayleigh-Taylor
<i>s</i>	Superficial, for single phase flow
<i>sim</i>	Regarding simulation
<i>sphere</i>	Sphere
<i>t</i>	Turbulence
<i>tot</i>	Total
<i>triangle</i>	Regarding triangle distribution
<i>turb</i>	Turbulence
<i>uniform</i>	Regarding uniform distribution

# List of Figures

2.1	Two-phase flow pattern for a liquid-gaseous-flow in adiabatic vertical pipe. a) bubble flow; b) plug flow; c) churn flow; d) wispy-annular flow; e) annular flow; f) spray or drop flow; Baehr and Stephan 2016 . . . . .	5
2.2	Two-phase flow pattern for a liquid-gaseous-flow in adiabatic horizontal pipe. a) bubble flow; b) plug flow; c) stratified flow; d) wavy flow; e) slug flow; f) annular flow; g) spray or drop flow Baehr and Stephan 2016 . . . . .	7
2.3	Flow pattern regions in two-phase flow, mass velocity of gas phase above ratio of liquid and gas mass velocities Baker 1958	9
2.4	Generalised Taitel and Dukler (1976) flow map for horizontal two-phase flow; figure by the author . . . . .	11
2.5	Schematic drawing of an Eckrohrkessel steam boiler; figure by the author . . . . .	14
2.6	Eckrohrkessel boiler types: (a) grate firing system single drum boiler, (b) fluidised bed single drum boiler, (c) tail end single drum boiler for waste incineration, (d) gas/oil burner bi drum boiler; ERK Eckrohrkessel GmbH 2018 . . . . .	16
2.7	Steam drum with natural steam/water separation and different steaming rates; see Kitto and Stultz (2005) . . . . .	19
2.8	Steam drum with natural steam/water separation and different inlet locations of; see Kitto and Stultz (2005) . . . . .	21

2.9	Eckrohrkessel baffle and scrubber drum internals 3D drawing: (a) Drum baffle internals for single drum boiler, (b) Drum baffle internals for bi drum boilers; ERK Eckrohrkessel GmbH 2018 . . . . .	22
2.10	Eckrohrkessel baffle and scrubber drum internals pictures at side: (a) longitudinal and side baffle plate arrangement, (b) side baffle plate and scrubber box for steam outlet at the top of the drum; ERK Eckrohrkessel GmbH 2018 . . . . .	23
2.11	Typical steam/water mechanical separators: (a) Conical cy- clone, (b) Curved arm, (c) horizontal cyclone seperator, (d) vertical cyclone separator; Kitto and Stultz 2005 . . . . .	24
2.12	Steam drum internals with three rows of cyclone separators; see Kitto and Stultz (2005) . . . . .	25
2.13	Local instant formulation of fluid density in time; figure by the author . . . . .	35
2.14	Local instant formulation of arbitrary variable with various time intervals; figure by the author . . . . .	36
2.15	Blending functions $f_b$ , $f_d$ and $f_{fs}$ regarding to 2.57; figure by the author . . . . .	49
2.16	Two-phase surface layer; upper and lower bounds are indicated with dashed lines; mean free surface is given with a solid line; Brocchini and Peregrine 2001 . . . . .	50
2.17	Schematic drawing of sphere in simple shear flow; figure by the author . . . . .	57
2.18	Distorted fluid particle with dimensions following Tomiyama et al. (2002a) . . . . .	60
2.19	Deformation of drops an bubbles in pure Water; Clift, Grace, and Weber 1978 . . . . .	61
2.20	Schematic drawing of drainage around a sphere near the wall; figure by the author . . . . .	62
2.21	FAD multiplier decreasing function; figure by the author . . .	64

3.1	Shape regimes for bubbles and drops in unhindered gravitational motion through liquids; Clift, Grace, and Weber 1978 . . . . .	81
3.2	Single particle drag coefficient by plotting equation for viscous regime drag coefficient and drag limits; figure by the author . . . . .	87
3.3	Drag coefficient for droplets and bubbles with 2 mm diameter in multiparticle system by plotting equation 3.43; air-water at 25 °C, 1 atm; figure by the author . . . . .	91
3.4	Maximum particle radius for droplets and bubbles in multiparticle system by plotting equation 3.48 and 3.47; air-water at 25 °C, 1 atm; figure by the author . . . . .	91
4.1	Example of NOW model CEL function; by the author . . . . .	98
4.2	Example of NOW model CEL constant; by the author . . . . .	98
4.3	Interfacial Area Density Implementation with RRSB distribution in Ansys CFX Mixture Model; by the author . . . . .	99
5.1	Steam drum flow pattern with natural steam/water separation; see Kitto and Stultz 2005 . . . . .	102
5.2	Fabre channel general experiment set-up scheme, see Fabre, Masbernat, and Suzanne (1987) . . . . .	104
5.3	Fabre channel CFD 2D geometry with dimensions for run reference 400 data (table 5.1); figure by the author . . . . .	106
5.4	Fabre channel CFD 2D mesh; figure by the author . . . . .	107
5.5	Fabre channel CFD model boundary conditions; figure by the author . . . . .	108
5.6	Fabre channel run reference 400 data (table 5.1) mesh study; normalised pressure gradient deviation (NPGD) over number of Elements; figure by the author . . . . .	114
5.7	Fabre channel run reference 400 data (table 5.1) mesh study; sum of normalised RMS kinetic energy, normalised RMS velocity, normalised water level and normalised RMS pressure gradient value for different mesh sizes; figure by the author . .	115

5.8	Fabre channel run reference 400 data (table 5.1) distribution function study; sum of normalised RMS kinetic energy, normalised RMS velocity, normalised water level and normalised RMS pressure gradient value for different simulation setups; figure by the author . . . . .	122
5.9	Fabre channel run reference 400 data (table 5.1) validation; sum of average normalised RMS kinetic energy, average normalised RMS velocity, normalised water level and average normalised RMS pressure gradient value for different cases; figure by the author . . . . .	127
5.10	Fabre channel run reference 400 data (table 5.1) validation; Liquid volume fraction at $x = 3\text{m}$ above the channel height Y for case F_000 and FV_010; figure by the author . . . . .	128
5.11	Fabre channel run reference 400 data (table 5.1) validation; Kinetic energy at $x = 3\text{m}$ above the channel height Y for case F_000 and FV_020; figure by the author . . . . .	130
5.12	Fabre channel run reference 400 data (table 5.1) validation; Velocity at $x = 3\text{m}$ above the channel height Y for case F_000 and FV_100; figure by the author . . . . .	132
5.13	Fabre channel run reference 400 data (table 5.1) validation; IAD times CD at $x = 3\text{m}$ above the channel height Y for case F_000 and FV_030; figure by the author . . . . .	133
5.14	Fabre channel run reference 400 data (table 5.1) validation; Kinetic energy at $x = 3\text{m}$ above the channel height Y for case F_000, FV_040 and FV_050; figure by the author . . . . .	134
5.15	Fabre channel run reference 400 data (table 5.1) validation; Drag force at $x = 3\text{m}$ above the channel height Y for case F_000, FV_060 and FV_070; figure by the author . . . . .	136
5.16	Fabre channel run reference 400 data (table 5.1) validation; Interface area density times drag coefficient at $x = 3\text{m}$ above the channel height Y for case F_000, FV_060 and FV_070; figure by the author . . . . .	137

5.17	Fabre channel run reference 400 data (table 5.1) validation; Liquid volume fraction at $x = 3\text{m}$ above the channel height Y for case F_000, FV_060 and FV_070; figure by the author . . .	138
5.18	Fabre channel run reference 400 data (table 5.1) validation; Drag force at $x = 3\text{m}$ above the channel height Y for case F_000 and FV_120; figure by the author . . . . .	140
5.19	Fabre channel run reference 400 data (table 5.1) validation; Liquid volume fraction at $x = 3\text{m}$ above the channel height Y for case F_000 and FV_120; figure by the author . . . . .	141
6.1	Hewitt and Owen (1987) experiment set-up scheme; see Hewitt and Owen 1987 . . . . .	147
6.2	Hewitt CFD model drawing with dimensions; figure by the author . . . . .	149
6.3	Hewitt CFD model; surface mesh; figure by the author . . .	150
6.4	Hewitt CFD model; 2D mesh at inlet; figure by the author . .	150
6.5	Hewitt CFD model; boundary conditions; figure by the author	151
6.6	Hewitt CFD model, Run No. 6; mass imbalances over iterations; figure by the author . . . . .	153
6.7	Hewitt CFD model pressure gradient over iterations (a) Run No. 1, (b) Run No. 6; figure by the author . . . . .	155
7.1	ERK steam drum internals schematic drawing; Schreiber, Hellwig, and Nowitzki 2017 . . . . .	159
7.2	Construction of the steam drum experiment; Schreiber, Hellwig, and Nowitzki 2017 . . . . .	162
7.3	Construction of the steam drum experiment feeding pipes; Schreiber, Hellwig, and Nowitzki 2017 . . . . .	163
7.4	Feeding pipes set 3 visual water level snapshot; case 500 L/h water and 25 m <sup>3</sup> /h; (a) mixture pipe in front of connection pipe G3.1, (b) mixture pipe behind connection pipe G3.2, (c) overflow pipe in front of connection pipe Ü3.1, (d) overflow pipe behind connection pipe Ü3.2; Schreiber, Hellwig, and Nowitzki 2017 . . . . .	165

7.5	Naming of feeding pipes in experiment steam drum regarding water content and flow pattern; Schreiber, Hellwig, and Nowitzki 2017 . . . . .	166
7.6	CFD Construction of the steam drum experiment with dimensions; Wehner, Hellwig, and Nowitzki 2017 . . . . .	168
7.7	3D drawing of the experiment steam drum; figure by the author	169
7.8	Mesh overview of the experiment steam drum cut; Coloured by volume size; figure by the author . . . . .	170
7.9	Mesh details of the experiment steam drum; Coloured by volume size, (a) steam drum, (b) steam drum stage 1, (c) distributor pipe, (d) orifice pipe; figure by the author . . . . .	171
7.10	Experiment steam drum simulation; Coloured by liquid volume size, feeding pipe (a) set 1, (b) set 2, (c) set 3; figure by the author . . . . .	177
7.11	Experiment steam drum simulation; Coloured by liquid volume fraction; cut planes through orifice pipes and feeding pipe set 3 and a detail of phase separation in orifice pipe; figure by the author . . . . .	179
8.1	Experiment steam drum simulation; Coloured by liquid volume fraction; Cut through orifice pipe and feeding pipe set 3; Advanced interface interaction; figure by the author . . . . .	185
C.1	Hewitt CFD model, exemplary 2m section of the vertical pipe, Run No. 1; coloured by Eötvös number, interface length scale, bubble blend function and liquid volume fraction; figure by the author . . . . .	226
C.2	Hewitt CFD model, exemplary 2m section of the vertical pipe, Run No. 6; coloured by Eötvös number, interface length scale, bubble blend function and liquid volume fraction; figure by the author . . . . .	227
D.1	Mesh of the experiment steam drum cut; Detail Steam Drum; Coloured by volume size; figure by the author . . . . .	229

D.2	Mesh of the experiment steam drum cut; Detail Steam Drum Stage 1; Coloured by volume size; figure by the author . . . . .	230
D.3	Mesh of the experiment steam drum cut; Detail Distributor; Coloured by volume size; figure by the author . . . . .	231
D.4	Mesh of the experiment steam drum cut; Detail Orifice Pipe; Coloured by volume size; figure by the author . . . . .	232

# List of Tables

2.1	Part of the nomenclature in Baker (1958) . . . . .	9
2.2	Comparison of Baehr and Stephan (2016) horizontal flow pattern (figure 2.2) and Baker (1958) flow map (figure 2.3) . . . . .	10
2.3	Drag coefficient correlations for particle model available in Ansys CFX; see Ansys 2016c . . . . .	44
5.1	Fabre channel experiment general data; Fabre, Masbernat, and Suzanne 1987 . . . . .	105
5.2	Fabre channel experiment water velocity and turbulence energy profile run reference 400 data (table 5.1); Fabre, Masbernat, and Suzanne 1987 . . . . .	105
5.3	Fabre channel experiment air velocity and turbulence energy profile run reference 400 data (table 5.1); Fabre, Masbernat, and Suzanne 1987 . . . . .	106
5.4	Fabre channel mesh study simulation model parameter . . . . .	112
5.5	Fabre channel mesh study pressure gradient and normalised pressure gradient deviation (NPGD); run reference 400 data (table 5.1) . . . . .	113
5.6	Fabre channel distribution study simulation cases overview . . . . .	120
5.7	Distribution function study results of average NPGD, NWLD, average NVD, average NKED, average liquid mass flow out of air outlet and the line average Sauter mean diameter at $x=3.5\text{ m}$ ; Column minimum value coloured in green and maximum in red; Fabre channel run reference 400 data (table 5.1) . . . . .	121
5.8	Fabre channel validation simulation cases overview . . . . .	125

5.9	Validation results of average NPGD, NWLD, average NVD, average NKED and average liquid mass flow out of air outlet (MF Liq); Column minimum value coloured in green and maximum in red; Fabre channel run reference 400 data (table 5.1) . . . . .	126
6.1	Hewitt vertical pipe experiment constant parameter; Hewitt and Owen 1987 . . . . .	146
6.2	Extract of Hewitt vertical pipe experiment results; observed flow regime and pressure gradient; Hewitt and Owen 1987 . .	147
6.3	Hewitt proof of concept results; Averaged NPGD, observed flow regime from experiment and CFD simulation . . . . .	154
7.1	Droplet mass flow out of experiment left and right steam drum side . . . . .	167
7.2	Steam drum experiment global mesh parameters . . . . .	168
7.3	Steam drum experiment local refinement mesh parameters . .	169
7.4	Steam drum simulation droplet mass flow at sides; water volume flow $0.5 \text{ m}^3/\text{h}$ , gas volume flow $25 \text{ m}^3/\text{h}$ , 1 atm . . . . .	175

# Bibliography

- Al-Sheikh, J. N., D. E. Saunders, and Robert S. Brodkey (1970). „Prediction of flow patterns in horizontal two-phase pipe flow“. In: *The Canadian Journal of Chemical Engineering* 48.1, pp. 21–29. DOI: [10.1002/cjce.5450480105](https://doi.org/10.1002/cjce.5450480105).
- Anderson, John David (1995). *Computational fluid dynamics: The basics with applications*. Internat. ed. McGraw-Hill series in aeronautical and aerospace engineering. New York: McGraw-Hill. ISBN: 0070016852.
- Ansys (2016a). *CFX-Pre User Guide 17.2*.
- (2016b). *CFX-Solver Modeling Guide*.
- (2016c). *CFX Theory Guide 17.2*.
- (2016d). *Fluent Theory Guide 17.2*.
- Antal, S. P., R. T. Lahey, and J. E. Flaherty (1991). „Analysis of phase distribution in fully developed laminar bubbly two-phase flow“. In: *International Journal of Multiphase Flow* 17.5, pp. 635–652. ISSN: 03019322. DOI: [10.1016/0301-9322\(91\)90029-3](https://doi.org/10.1016/0301-9322(91)90029-3). URL: <http://www.sciencedirect.com/science/article/pii/0301932291900293>.
- Apte, S. V., M. Gorokhovski, and P. Moin (2003). „LES of atomizing spray with stochastic modeling of secondary breakup“. In: *International Journal of Multiphase Flow* 29, pp. 1503–1522. ISSN: 03019322.
- Avdeev, Alexander A. (2016). *Bubble Systems*. Mathematical Engineering. Cham and s.l.: Springer International Publishing. ISBN: 9783319292861.

- DOI: 10.1007/978-3-319-29288-5.  
URL: <http://dx.doi.org/10.1007/978-3-319-29288-5>.
- Aybers, N. M. and A. Tapucu (1969). „Studies on the drag and shape of gas bubbles rising through a stagnant liquid“.  
In: *Wärme - und Stoffübertragung* 2.3, pp. 171–177. ISSN: 1432-1181.  
DOI: 10.1007/BF00751164.  
URL: <https://doi.org/10.1007/BF00751164>.
- Baehr, Hans Dieter and Karl Stephan (2016).  
*Wärme- und Stoffübertragung*. 9., aktualisierte Auflage. Lehrbuch.  
Berlin and Heidelberg: Springer Vieweg. ISBN: 3662496763.
- Baker, Ovid (1954). „Simultaneous Flow of Oil and Gas“.  
In: *Oil and Gas Journal* 53, pp. 185–195.
- (1958). „Multiphase flow in pipelines“. In: *Pipeline News*, pp. 156–167.
- Barnea, D. (1987). „A unified model for predicting flow-pattern transitions for the whole range of pipe inclinations“.  
In: *International Journal of Multiphase Flow* 13.1, pp. 1–12.  
ISSN: 03019322. DOI: 10.1016/0301-9322(87)90002-4.
- Barnea, Dvora et al. (1980).  
„Flow pattern transition for gas-liquid flow in horizontal and inclined pipes. Comparison of experimental data with theory“.  
In: *International Journal of Multiphase Flow* 6.3, pp. 217–225.  
ISSN: 03019322. DOI: 10.1016/0301-9322(80)90012-9.
- Bošnjaković, Fran and Karl Friedrich Knoche (1988).  
*Technische Thermodynamik*. 7., neubearb. und erw. Aufl. Vol. 11,1.  
Wärmelehre und Wärmewirtschaft.  
Leipzig: Dt. Verl. für Grundstoffindustrie. ISBN: 3342003189.
- Brocchini, Maurizio and D. H. Peregrine (2001). „The dynamics of strong turbulence at free surfaces. Part 2. Free-surface boundary conditions“.  
In: *Journal of Fluid Mechanics* Volume 449, pp. 255–290.  
DOI: 10.1017/S0022112001006024.
- Brodkey, Robert. S. (2005). *The Phenomena of Fluid Motions*.  
Ohio, USA: Brodkey Publishing. ISBN: 0972663576.

- Burns, Alan et al. (2004).
- 5th International Conference on Multiphase Flow: The Favre Averaged Drag Model for Turbulent Dispersion in Eulerian Multi-Phase Flows.*  
Yokohama, Japan.
- Cheremisinoff, Nicholas P. and Ramesh Gupta, eds. (1983).
- Handbook of fluids in motion.* Boston: Butterworths. ISBN: 0250404583.
- Clift, Roland, J. R. Grace, and M. E. Weber (1978).
- Bubbles, drops, and particles.* New York: Academic Press.  
ISBN: 012176950X.
- Drew, D. A. and R. T. Lahey (1987). „The virtual mass and lift force on a sphere in rotating and straining inviscid flow“.  
In: *International Journal of Multiphase Flow* 13.1, pp. 113–121.  
ISSN: 03019322. DOI: 10.1016/0301-9322(87)90011-5. URL: <http://www.sciencedirect.com/science/article/pii/0301932287900115>.
- Dukler, A. E. and Yehuda Taitel (1986). „Flow Pattern Transitions in Gas-Liquid Systems: Measurement and Modeling“.  
In: *Multiphase Science and Technology*. Ed. by Geoffrey Frederick Hewitt, Jean-Marc Delhaye, and Novak Zuber.  
Vol. 2. Springer-Verlag Berlin. ISBN: 3-540-16408-1.
- Egorov, Yury (2004). *Validation of CFD codes with PTS-relevant test cases.*  
Ed. by EVOL-ECORA-D07.
- Epple, Bernd et al., eds. (2012).
- Simulation von Kraftwerken und Feuerungen.* 2., erw. und korr. Aufl.  
Wien: Springer. ISBN: 9783709111819.
- ERK Eckrohrkessel GmbH (2018). *internal raw material.*
- Ervin, E. A. and G. Tryggvason (1997).  
„The Rise of Bubbles in a Vertical Shear Flow“.  
In: *Journal of Fluids Engineering* 119.2, pp. 443–449. ISSN: 0098-2202.  
DOI: 10.1115/1.2819153.  
URL: <http://dx.doi.org/10.1115/1.2819153>.
- Fabre, J., L. Masbernat, and C. Suzanne (1987).  
„Stratified Flow, Part I: Local Structures“.  
In: *Multiphase Science and Technology*. Ed. by

- Geoffrey Frederick Hewitt, Jean-Marc Delhaye, and Novak Zuber.  
 Vol. 3. Springer-Verlag Berlin, pp. 285–301. ISBN: 3-540-17791-4.
- FDBR (2013). *FDBR-Handbuch: Wärme- und Strömungstechnik*.  
 FDBR Fachverband Dampfkessel-, Behälter- und Rohrleitungsbau e.V.
- Flügge, Siegfried et al. (1959). *Strömungsmechanik I: Fluid dynamics I*.  
 Vol. Bd. VIII/1. Handbuch der Physik Encyclopedia of physics.  
 Berlin, Göttingen, and Heidelberg: Springer.
- Govier, G. W. and M. M. Omer (1962).  
 „The Horizontal Pipeline Flow of Air-Water Mixtures“.  
 In: *The Canadian Journal of Chemical Engineering* 40, pp. 93–104.  
 DOI: 10.1002/cjce.5450400303.
- Griffith, Peter and Graham B. Wallis (1961). „Two-Phase Slug Flow“.  
 In: *Journal of Heat Transfer* 83.3, pp. 307–318.  
 DOI: 10.1115/1.3682268.  
 URL: <http://dx.doi.org/10.1115/1.3682268>.
- Harlow, Francis H. and Anthony A. Amsden (1975).  
 „Numerical Calculation of Multiphase Fluid Flow“.  
 In: *Journal of Computational Physics* Vol 17, pp. 19–52.
- Harmathy, Tibor Z. (1960). „Velocity of large drops and bubbles in media of infinite or restricted extent“.  
 In: *AICHE Journal* Vol. 6.2, pp. 281–288.
- Hayter, Anthony J. (2007).  
*Probability and statistics for engineers and scientists*. 3 ed.  
 International student edition. Pacific Grove: Duxbury.  
 ISBN: 9780495108788.
- Hewitt, Geoffrey Frederick and D. G. Owen (1987).  
 „Pressure Drop and Entrained Fraction in Fully Developed Flow“.  
 In: *Multiphase Science and Technology*. Ed. by  
 Geoffrey Frederick Hewitt, Jean-Marc Delhaye, and Novak Zuber.  
 Vol. 3. Springer-Verlag Berlin, pp. 145–154. ISBN: 3-540-17791-4.
- Höhne, Thomas (2009). „Experiments and Numerical Simulations of Horizontal Two Phase Flow Regimes“. In: *Seventh International Conference on CFD in the Minerals and Process Industries*.

- Höhne, Thomas and Christophe Vallée (2010).  
 „Experiments and Numerical Simulations of Horizontal Two-Phase Flow Regimes Using an Interfacial Area Density Model“. In: *The Journal of Computational Multiphase Flows* 2.3, pp. 131–143.  
 DOI: 10.1260/1757-482X.2.3.131.  
 URL: <https://doi.org/10.1260/1757-482X.2.3.131>.
- Huhn, Jörg and Joachim Wolf (1975).  
*Zweiphasenströmung: Gasförmig/flüssig.* 1. Aufl. Leipzig: Fachbuchverl. HZDR and Ansys, eds. (2016).
- 14th Multiphase Flow Conference and Short Course.*
- Ishii, Mamoru and Takashi Hibiki (2006).  
*Thermo-fluid Dynamics of Two-Phase Flow.* 1. Ed. Berlin: Springer US.  
 ISBN: 0387283218.
- Ishii, Mamoru and Novak Zuber (1979). *Drag coefficient and relative velocity in bubbly, droplet or particulate flows: Drag coefficient and relative velocity in bubbly, droplet or particulate flows.* New York: American Institute of Chemical Engineers.
- Kandlikar, Satish G., ed. (1999).  
*Handbook of phase change: Boiling and condensation.* Philadelphia, Pa.: Taylor & Francis. ISBN: 1560326344. URL: <http://www.loc.gov/catdir/enhancements/fy0653/99026754-d.html>.
- Kitto, John B. and Stultz, eds. (2005). *Steam: Its generation and use.* 41. ed., 1. print. Barberton, Ohio: Babcock & Wilcox. ISBN: 0963457012.
- Kolev, Nikolay Ivanov (2012).  
*Multiphase Flow Dynamics 2: Mechanical Interactions.* Berlin, Heidelberg: Springer Berlin Heidelberg. ISBN: 9783642205972.  
 DOI: 10.1007/978-3-642-20598-9.  
 URL: <http://dx.doi.org/10.1007/978-3-642-20598-9>.
- Kotz, Samuel and Johan René van Dorp (2004).  
*Beyond beta: Other continuous families of distributions with bounded support and applications.* Singapore and London: World Scientific.  
 ISBN: 9789812561152. URL: <http://search.ebscohost.com/login.aspx?direct=true&scope=site&db=nlebk&db=nlabk&AN=167309>.

- Krepper, Eckhard (1999). *HZDR Annual Report 1999: CFD Simulations of a Bubbly Flow in a Vertical Pipe*. Ed. by F. Weiß and U. Rindelhard. Dresden.
- Lockhart, R. and R. Martinelli (1949). „Proposed correlation of data for isothermal two-phase, two-component flow in pipes“. In: *Chemical Engineering Progress* 45.1, pp. 39–48.
- Lucas, Dirk and Eckhard Krepper (2007). *CFD models for polydisperse bubbly flows*. Vol. 486. Wissenschaftlich-technische Berichte / FZD, Forschungszentrum Dresden-Rossendorf. Dresden: FZD.
- Luo, Hean and Hallvard F. Svendsen (1996). *Theoretical model for drop and bubble breakup in turbulent dispersions: Theoretical model for drop and bubble breakup in turbulent dispersions*. New York: American Institute of Chemical Engineers.
- Mahaffy, J. et al. (2015). *Best Practice Guidelines for the Use of CFD in Nuclear Reactor Safety Application - Revision: JT03370465; OECD Nuclear Energy Agency (NEA) 2015*.
- Mayr, Fritz and Thomas Gritsch, eds. (1997). *Handbuch der Kesselbetriebstechnik: Kraft- und Wärmeerzeugung in Praxis und Theorie*. 7., erg. und verb. Aufl. Gräfelfing: Resch. ISBN: 3930039133.
- Mishima, Kaichiro and Mamoru Ishii (1984). „Flow Regime Transition Criteria for Upward Two-Phase Flow in Vertical Tubes“. In: *International Journal of Heat and Mass Transfer* 27.5, pp. 723–737.
- Pellacani, Filippo (2012). *Development and Validation of Bubble Breakup and Coalescence Constitutive Models for the One-Group Interfacial Area Transport Equation*. München.
- Porombka, P. and T. Höhne (2015). „Drag and turbulence modelling for free surface flows within the two-fluid Euler–Euler framework“. In: *Chemical Engineering Science* 134, pp. 348–359. ISSN: 00092509. DOI: [10.1016/j.ces.2015.05.029](https://doi.org/10.1016/j.ces.2015.05.029).
- Prof. Dr. J. Tomas (2014). „Mechanical Process Engineering - Particle Technology Disperse Systems - Script“.

- Prosperetti, A. and A.V. Jones (1984). „Pressure forces in disperse two-phase flow“. In: *International Journal of Multiphase Flow* 10.4, pp. 425–440. ISSN: 03019322. DOI: 10.1016/0301-9322(84)90054-5.
- Reitz, Rolf D. (1987). „Modeling atomization processes in high-pressure vaporizing sprays“. In: *Atomisation Spray Technology* 3, pp. 309–337.
- Reitz, Rolf D. and Jennifer C. Beale (1999). „MODELING SPRAY ATOMIZATION WITH THE KELVIN-HELMHOLTZ/RAYLEIGH-TAYLOR HYBRID MODEL“. In: *Atomization and Sprays* 9.6, pp. 623–650. ISSN: 1044-5110.
- Roscoe, R. (1952). „The viscosity of suspensions of rigid spheres“. In: *British Journal of Applied Physics* Volume 3.Issue 8, pp. 267–269.
- Saffman, P. G. (1965). „The lift on a small sphere in a slow shear flow“. In: *Journal of Fluid Mechanics* 22.2, pp. 385–400. DOI: 10.1017/S0022112065000824.
- Schreiber, Simon, Udo Hellwig, and Mario Nowitzki (2017). *Konstruktion, Aufbau und Erprobung zur Trennung von Zweiphasengemischen*. Wildau.
- Stieß, Matthias (2009). *Mechanische Verfahrenstechnik - Partikeltechnologie 1*. 3., vollst. neu bearb. Aufl. Springer-Lehrbuch. Berlin, Heidelberg: Springer Berlin Heidelberg. ISBN: 9783540325512. DOI: 10.1007/978-3-540-32552-9. URL: <http://site.ebrary.com/lib/alltitles/docDetail.action?docID=10257925>.
- Taitel, Yehuda, Dvora Bornea, and A. E. Dukler (1980). „Modelling flow pattern transitions for steady upward gas-liquid flow in vertical tubes“. In: *AICHE Journal* 26.3, pp. 345–354. DOI: 10.1002/aic.690260304.
- Taitel, Yemada and A. E. Dukler (1976). *A model for predicting flow regime transitions in horizontal and near horizontal gas-liquid flow: A model for predicting flow regime transitions in horizontal and near horizontal gas-liquid flow*. New York: American Institute of Chemical Engineers.

- Taylor, G. I. (1932). „The Viscosity of a Fluid Containing Small Drops of Another Fluid“. In: *Royal Society* Volume 138.issue 834, pp. 41–48.
- Tomiyama, A., ed. (2002). *SINGLE BUBBLES IN STAGNANT LIQUIDS AND IN LINEAR SHEAR FLOWS*.
- Tomiyama, A. et al. (2002a). „Terminal velocity of single bubbles in surface tension force dominant regime“. In: *International Journal of Multiphase Flow* 28.9, pp. 1497–1519. ISSN: 03019322. DOI: 10.1016/S0301-9322(02)00032-0. URL: <http://www.sciencedirect.com/science/article/pii/S0301932202000320>.
- Tomiyama, Akio et al. (2002b). „Transverse migration of single bubbles in simple shear flows“. In: *Chemical Engineering Science* 57, pp. 1849–1858. ISSN: 00092509.
- Vallée, Christophe and Thomas Höhne (2006). „CFD VALIDATION OF STRATIFIED TWO-PHASE FLOWS IN A HORIZONTAL CHANNEL“. In: *Annual Report 2006*. Dresden, pp. 33–38.
- Vallée, Christophe et al. (2008). „Experimental investigation and CFD simulation of horizontal stratified two-phase flow phenomena“. In: *Nuclear Engineering and Design* 238.3, pp. 637–646. ISSN: 0029-5493. DOI: 10.1016/j.nucengdes.2007.02.051.
- Versteeg, Henk K. and Weeratunge Malalasekera (2007). *An introduction to computational fluid dynamics: The finite volume method*. 2. ed., [Nachdr.] Harlow: Pearson/Prentice Hall. ISBN: 9780131274983.
- Wallis, Graham B. (1969). *One-dimensional two-phase flow*. New York: McGraw-Hill. ISBN: 0070679428.
- Wehner, Michelle, Udo Hellwig, and Mario Nowitzki (2017). *Numerische Simulation des Stoffgemisches Luft-Wasser im Modell einer technischen Dampftrommel*.
- Wellek, R. M., A. K. Agrawal, and A. H. P. Skelland (1966). „Shape of liquid drops moving in liquid media“. In: *AIChE Journal* 12.5, pp. 854–862. ISSN: 0001-1541. DOI: 10.1002/aic.690120506.

- Winnikow, S. and B. T. Chao (1966). „Droplet Motion in Purified Systems“. In: *The Physics of Fluids* 9.1, pp. 50–61. ISSN: 0031-9171. DOI: 10.1063/1.1761532.
- Wu, Benjamin et al. (2017). „A critical review of flow maps for gas-liquid flows in vertical pipes and annuli“. In: *Chemical Engineering Journal* 326, pp. 350–377. ISSN: 1385-8947. DOI: 10.1016/j.cej.2017.05.135. URL: <http://www.sciencedirect.com/science/article/pii/S1385894717308938>.
- XIN, J., L. RICART, and R. D. REITZ (1998). „Computer Modeling of Diesel Spray Atomization and Combustion“. In: *Combustion Science and Technology* 137.1-6, pp. 171–194. DOI: 10.1080/00102209808952050. URL: <https://doi.org/10.1080/00102209808952050>.
- Zogg, Martin (1993). *Einführung in die mechanische Verfahrenstechnik: Mit 29 Tabellen und 32 Berechnungsbeispielen*. 3., überarb. Aufl. Stuttgart: Teubner. ISBN: 3519163195.

# Acknowledgements

I could not have written this thesis without the support from Prof. Dr.-Ing Udo Hellwig and Prof. Thomas Mirre. They gave me inspiration and had my back.

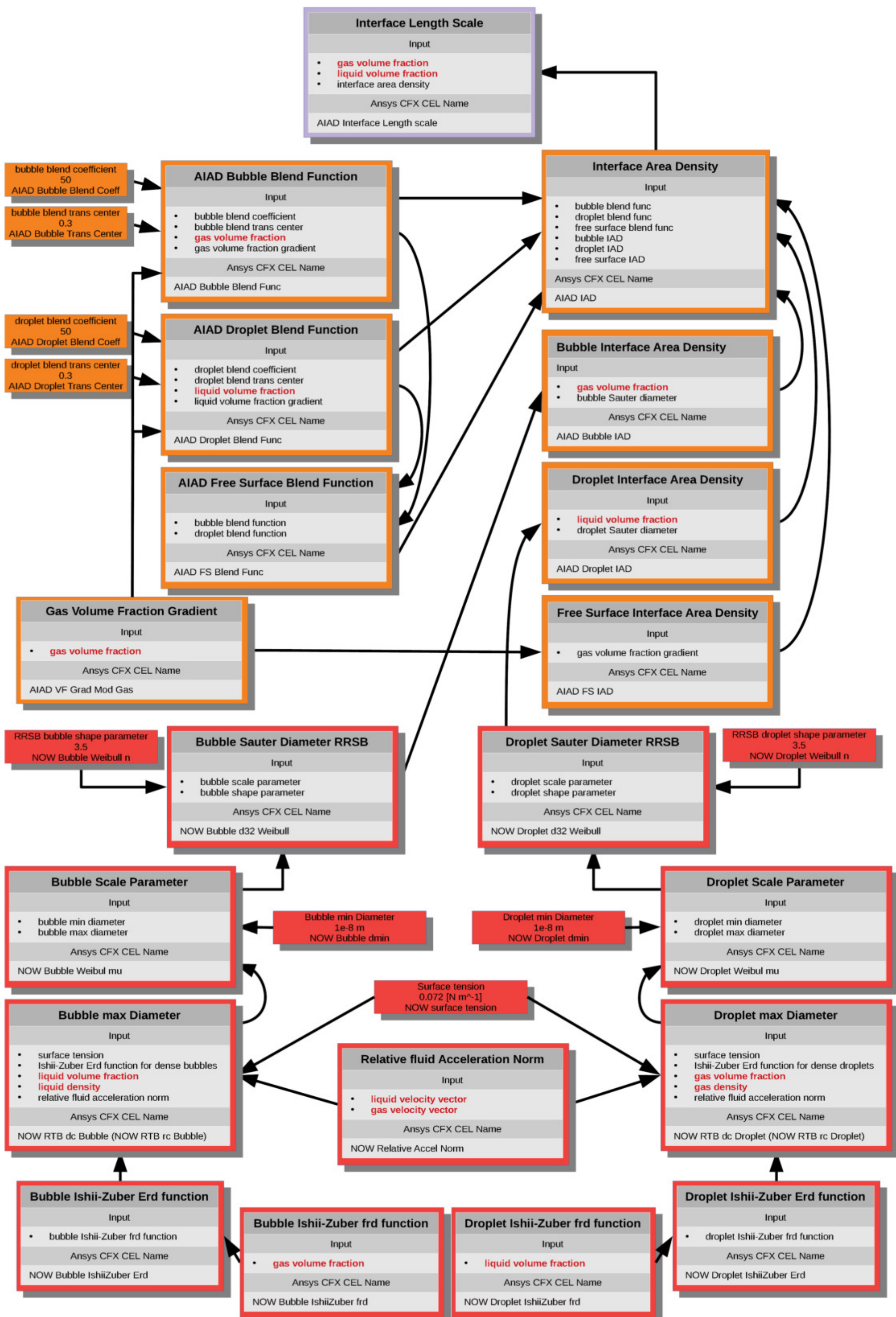
Many thanks to my supervisors Prof. Dr.-Ing. Fabian Mauß and Prof. Dr.-Ing. Hans-Joachim Krautz and all the people in the background who supported me.

Dr. Thomas Höhne from the HZDR very kindly provided the source code for the AIAD model.

# Appendices

## **Appendix A**

### **Interface Area Density Implementation Flowchart**

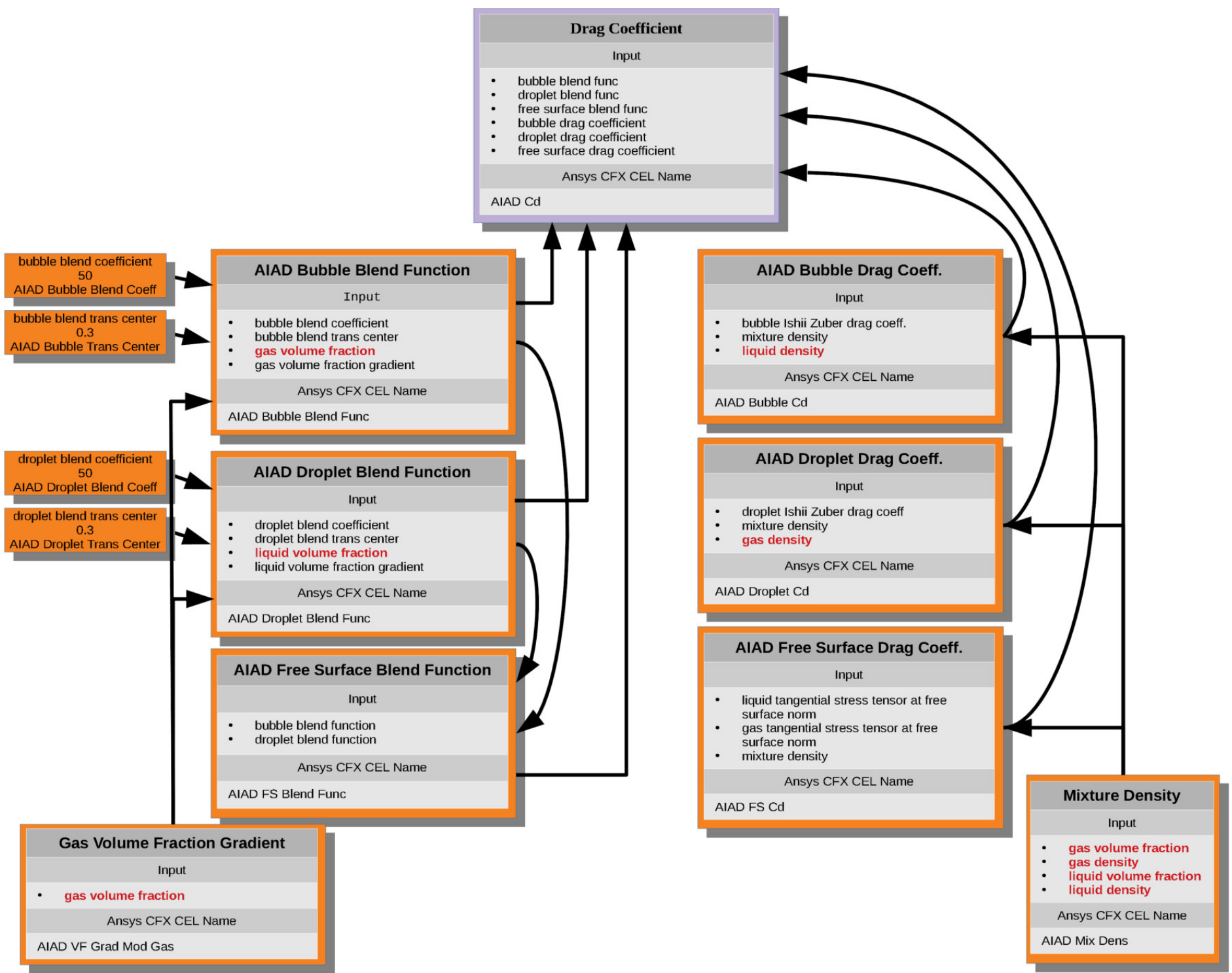


Interfacial Area Density Implementation in Ansys CFX Mixture Model; by the author



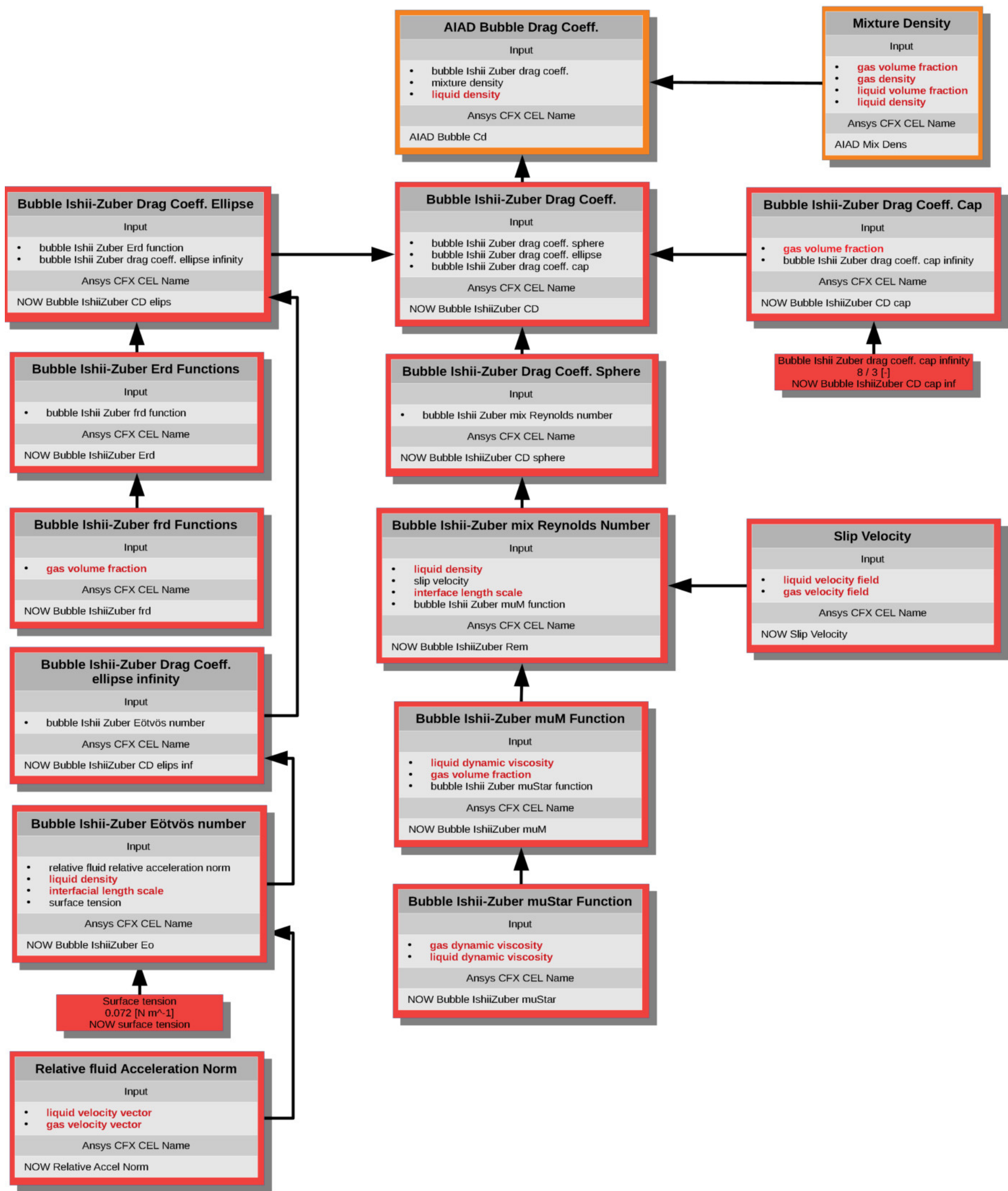
## **Appendix B**

### **Ishii Zuber Drag Model Implementation Flowchart**



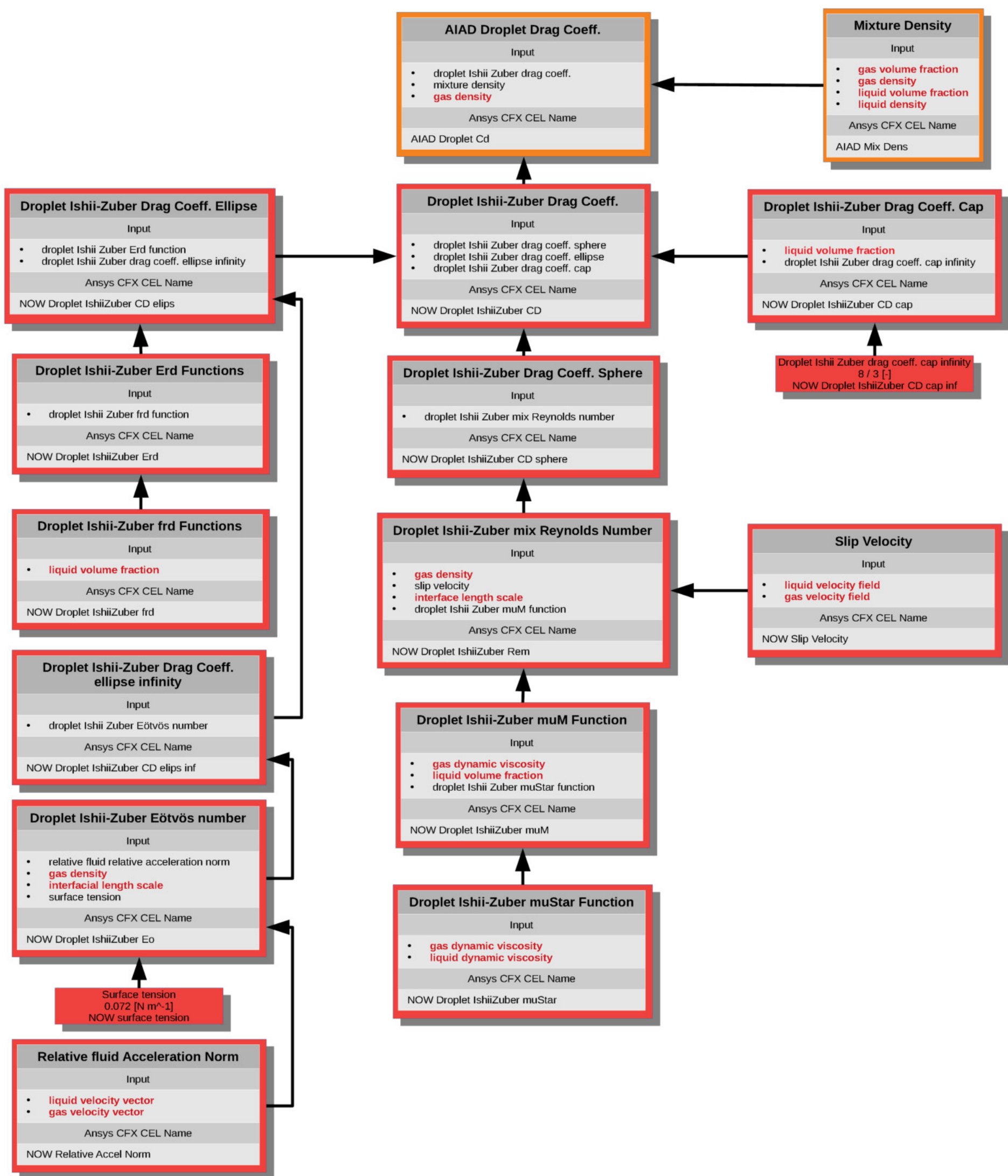
Ishii Zuber drag model implementation in CFX Mixture model; overview





Ishii Zuber drag model implementation in CFX Mixture model; for bubbles





Ishii Zuber drag model implementation in CFX Mixture model; for droplets



## **Appendix C**

### **Proof of Concept Hewitt Experiment**

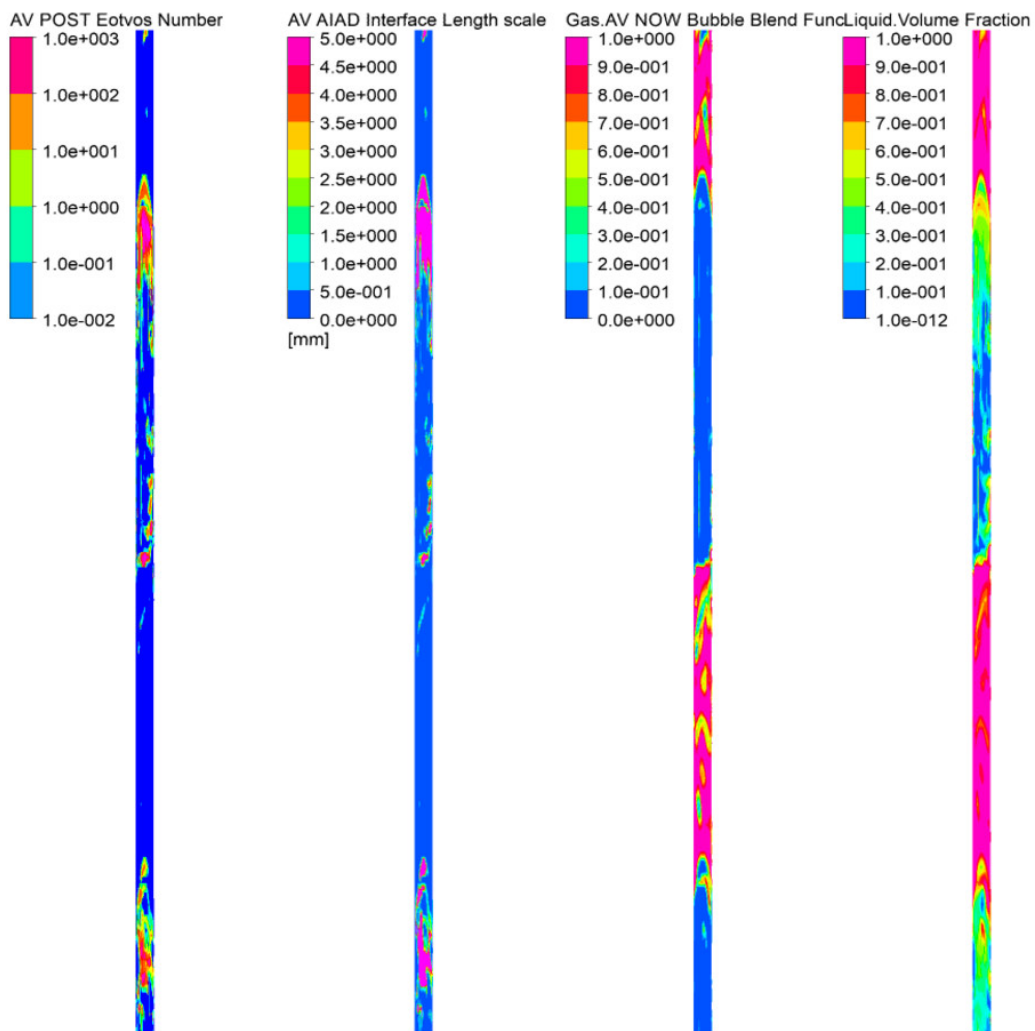


Figure C.1: Hewitt CFD model, exemplary 2m section of the vertical pipe, Run No. 1; coloured by Eötvös number, interface length scale, bubble blend function and liquid volume fraction; figure by the author

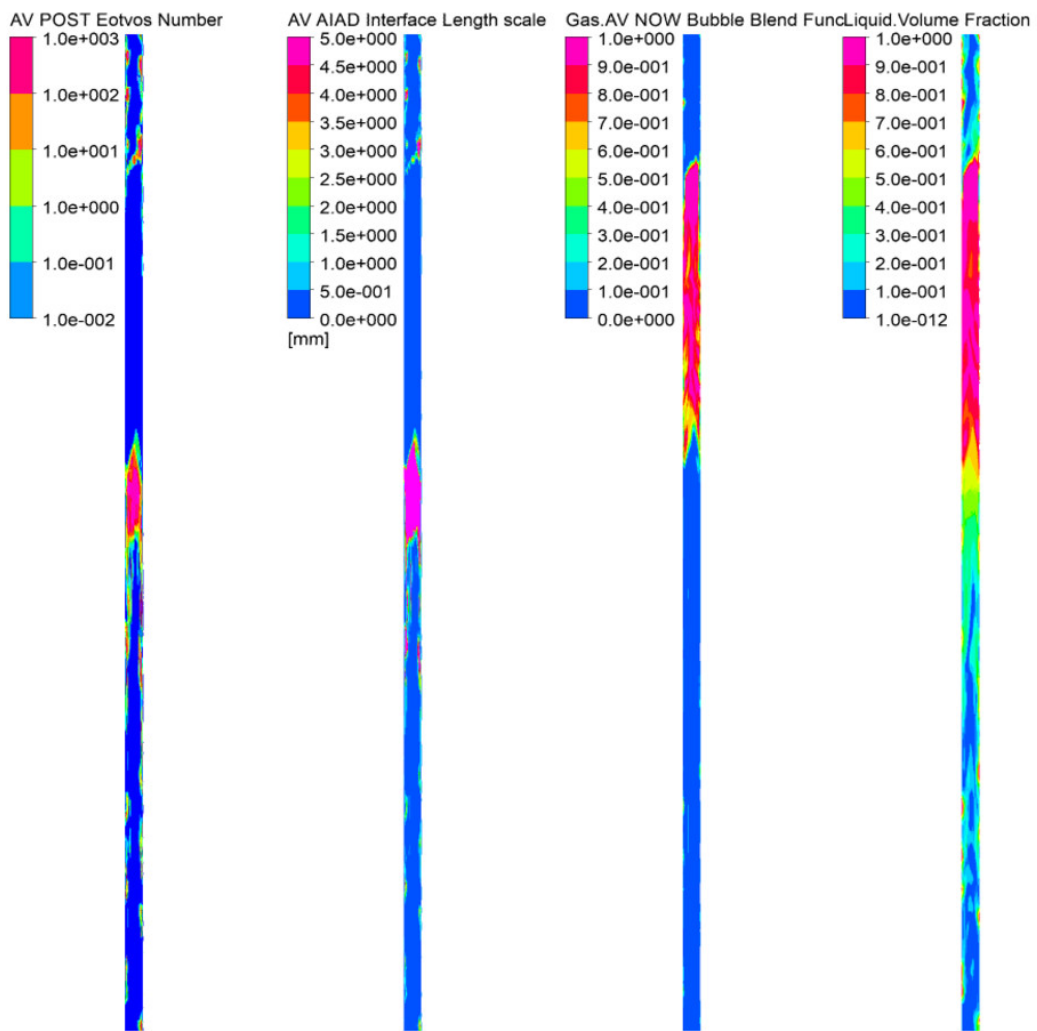


Figure C.2: Hewitt CFD model, exemplary 2m section of the vertical pipe, Run No. 6; coloured by Eötvös number, interface length scale, bubble blend function and liquid volume fraction; figure by the author

# **Appendix D**

## **Steam Drum Experiment**

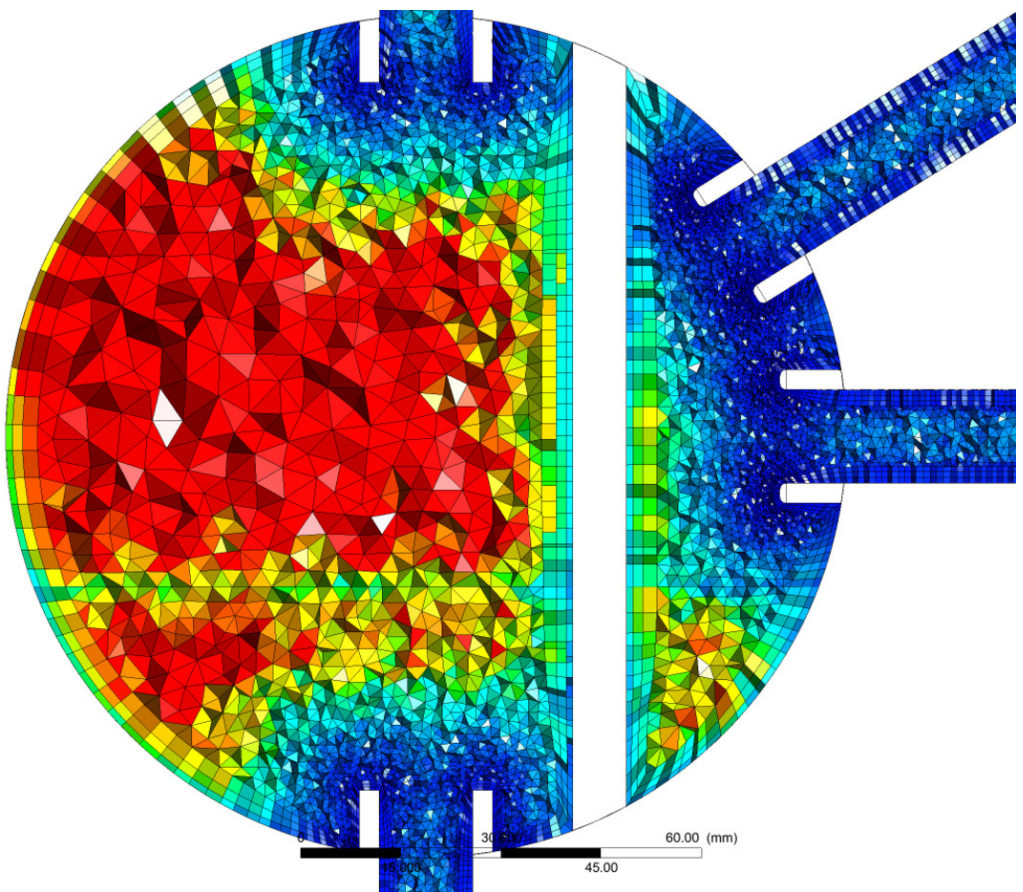


Figure D.1: Mesh of the experiment steam drum cut; Detail Steam Drum;  
Coloured by volume size; figure by the author

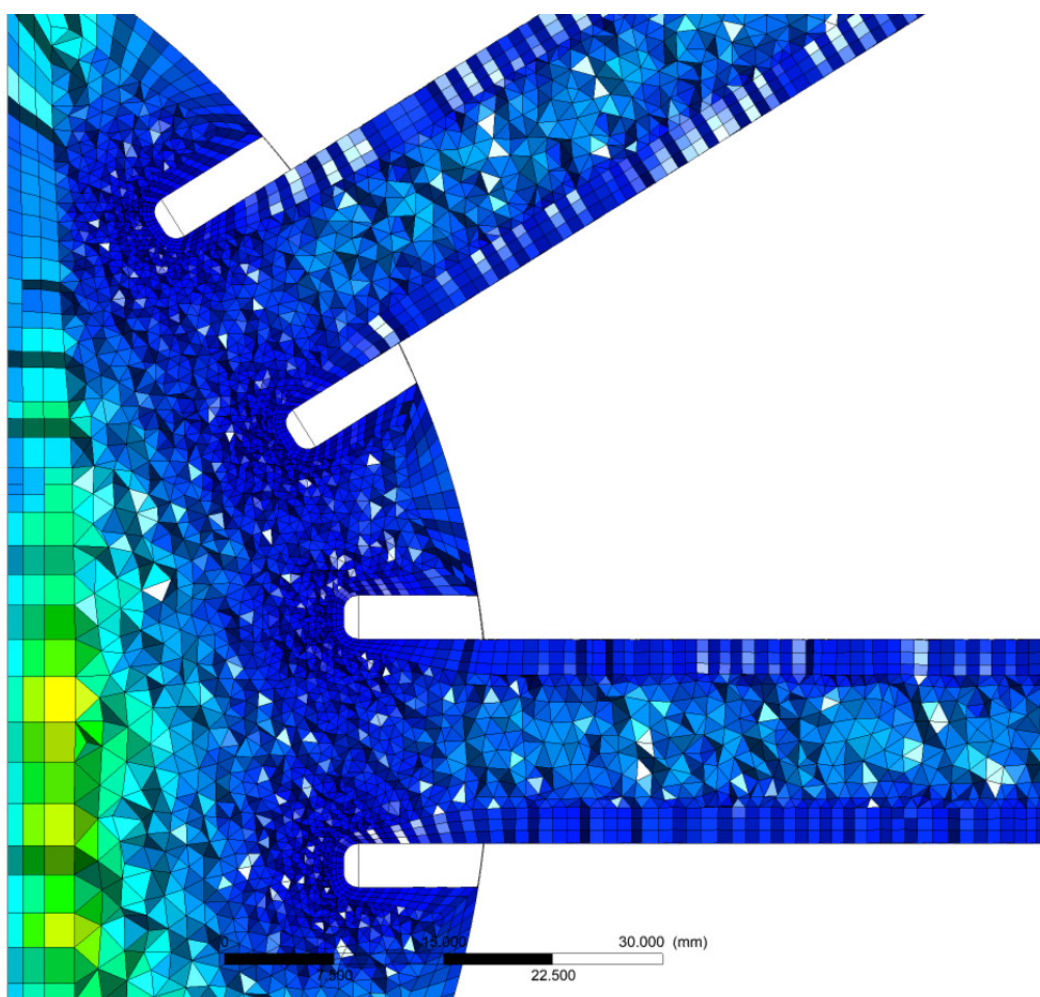


Figure D.2: Mesh of the experiment steam drum cut; Detail Steam Drum Stage 1; Coloured by volume size; figure by the author

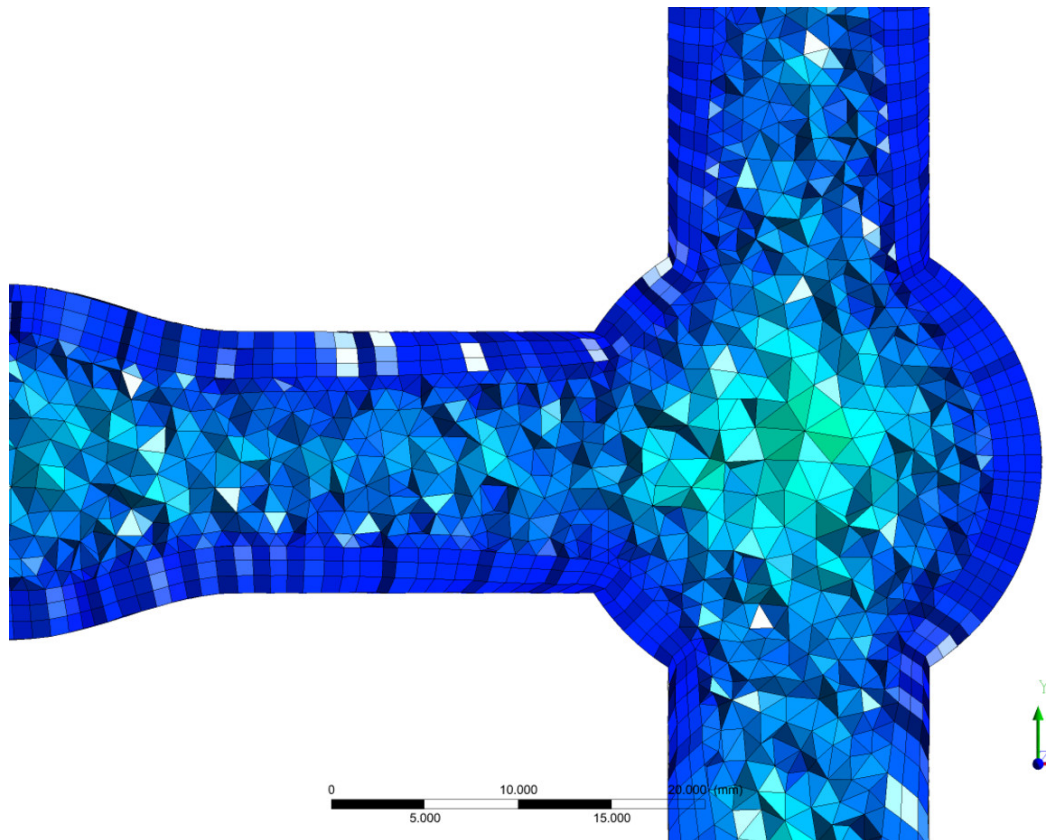


Figure D.3: Mesh of the experiment steam drum cut; Detail Distributor;  
Coloured by volume size; figure by the author

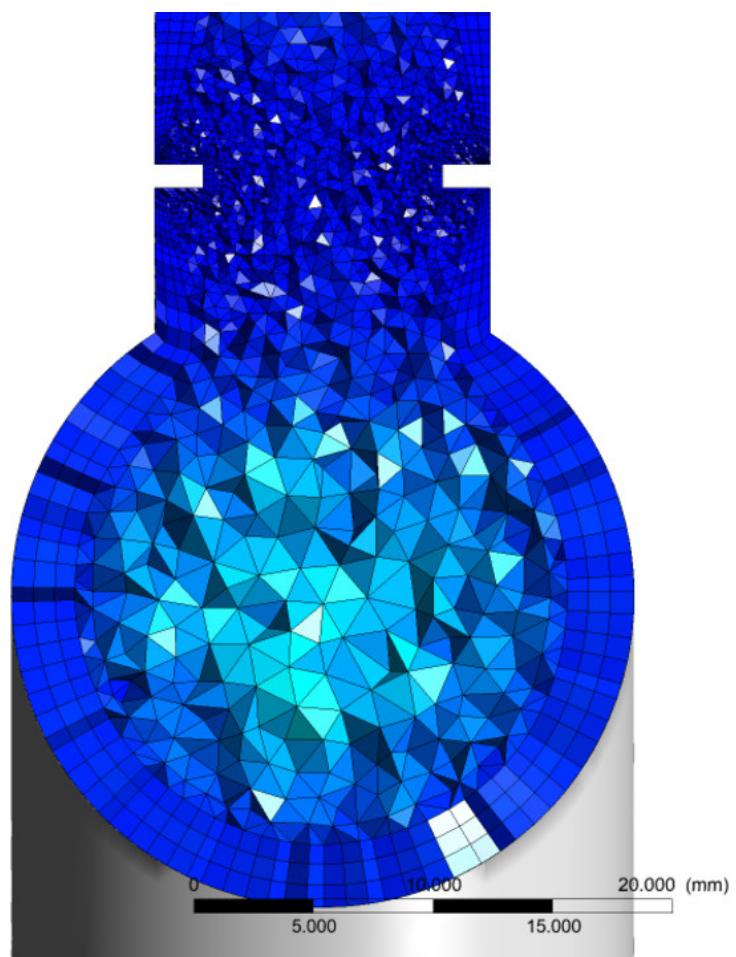


Figure D.4: Mesh of the experiment steam drum cut; Detail Orifice Pipe;  
Coloured by volume size; figure by the author